Gamow-Teller strength in (n,p) charge exchange on ^{31}P

R. M. Sedlar,[1] T. P. Gorringe,[1] W. P. Alford,[4] D. A. Beatty,[2] J. Campbell,[3] H. T. Fortune,[2] P. Hui,[2] D. A. Hutcheon,[3] R. B. Ivie,[2] K. P. Jackson,[3] A. G. Ling,[3] Z. Mao,[2] M. G. McKinzie,[2] B. Siebels,[1] D. A. Smith,[2] P. Walden,[3] and S. Yen[3]
[1]*Department of Physics and Astronomy, University of Kentucky, Lexington, Kentucky 40506*
[2]*Department of Physics and Astronomy, University of Pennsylvania, Philadelphia, Pennsylvania 19104*
[3]*TRIUMF, 4004 Wesbrook Mall, Vancouver, British Columbia, Canada V6T 2A3*
[4]*Department of Physics, University of Western Ontario, London, Ontario, Canada N6A 3K7*
(Received 28 September 1998)

Using the charge exchange facility and second arm spectrometer at TRIUMF, we have measured the ^{31}P(n,p) double differential cross section for 198 MeV incident neutrons, at scattering angles of 0–30°, and excitation energies up to 30 MeV. Via a multipole decomposition analysis we have extracted both the Gamow-Teller strength distribution and the GT transition probabilities to low-lying ^{31}Si bound states. Comparison to a shell model calculation, using the full $1s$-$0d$ space and universal SD interaction, shows reasonable agreement in the strength distribution, but reduced summed strength in the experiment ($\Sigma B_{\mathrm{GT}}=2.32\pm0.20$ for $E_x \leqslant 10$ MeV) relative to the theory ($\Sigma B_{\mathrm{GT}}=3.33$ for $E_x \leqslant 10$ MeV). We discuss the role of configuration mixing and Pauli blocking on the $^{31}P \rightarrow {}^{31}$Si GT strength distribution. [S0556-2813(99)06602-9]

PACS number(s): 25.40.Kv, 23.40.−s, 24.30.Cz, 27.30.+t

I. INTRODUCTION

The (p,n) and (n,p) charge exchange reactions, at forward angles and medium energies, are established probes of Gamow-Teller (GT) excitations in nuclei [1,2]. Their use to map the quenching of GT strength is a milestone topic in nuclear physics (e.g. [3]). Their use to determine the GT transition probabilities of selected GT transitions has proved valuable in fields including supernova dynamics [4–6], neutrino detection [7], and double β-decay [8].

The long-standing question of the in-medium value of the nucleon's induced pseudoscalar coupling is attracting continued attention [9–14]. Although both the induced pseudoscalar coupling (g_p) and the familiar axial coupling (g_a) formally govern the nucleon's weak axial current, only in μ-capture, and not in β-decay, are there measurable effects of g_p. A recent experiment to extract g_p from GT transitions in muonic ^{23}Na [12] greatly profited from independent knowledge of the relevant GT matrix elements determined via ^{23}Na(n,p) charge exchange data [15]. An on-going experiment to extract g_p from GT transitions in muonic ^{31}P [16] partially motivated the present work.

Gamow-Teller transitions have special significance in nuclear structure. Since the GT operator acts on spin-isopin coordinates only, neither changing a nucleon's principal or orbital quantum numbers, GT strength distributions provide a sensitive test of shell model calculations. In particular, determinations of GT strength via (n,p) reactions on $N>Z$ nuclei are especially sensitive to Pauli blocking, configuration mixing, and the residual interaction [28]. Given the paucity of (n,p) data on $N>Z$ nuclei in the $1s$-$0d$ shell [15], a comparison of measured and calculated $^{31}\mathrm{P} \rightarrow {}^{31}$Si GT strength distributions is of interest.

We report measurements of the double differential cross section for the ^{31}P(n,p) reaction with 198 MeV incident neutrons, scattering angles of 0–30°, and excitation energies up to 30 MeV. Through a multipole decomposition analysis of the cross section data we extract the GT strength distribution. Section II describes the experimental setup, Sec. III the determination of the (n,p) cross section, Secs. IV and V the extraction of the GT strength, and Sec. VI the comparison to various shell model calculations. We summarize in Sec. VII.

II. EXPERIMENTAL SETUP

The measurement was conducted at TRIUMF using the charge exchange facility and the second arm spectrometer (for details see Refs. [2,17] and [18], respectively).

The 198 MeV neutron beam is derived from the 200 MeV proton beam via the (p,n) reaction on a ^{7}Li foil. Downstream of the ^{7}Li foil a sweeping magnet separates the protons from the neutrons, and downstream of the sweeping magnet a veto scintillator (FEV) identifies any proton contamination in the neutron beam. The resulting neutron beam is nearly monenergetic [^{7}Li$(p,n)^7$Be* breakup yields a small low-energy tail], with an on-target flux of $\sim 10^6$ n/s.

The (n,p) target assembly [17] comprised an interleaved array of eight wire chambers and six target elements [five ^{31}P targets elements and one CH_2 target element denoted $(^{31}\mathrm{P})^5 \cdot \mathrm{CH}_2$]. The ^{31}P targets were red phosphorus powder sandwiched between thin Mylar foils and epoxyed onto aluminum support frames. They were assembled under either an argon or a nitrogen atmosphere, avoiding H_2O absorption by the ^{31}P targets and minimizing ^{1}H(n,p) contamination of the ^{31}P(n,p) spectra. The ^{31}P targets were 110 mg/cm^2 in thickness and 4×6 cm^2 in cross section. The wire chamber hit pattern identified the struck target element and permitted correction for proton energy loss in the target layers downstream. The CH_2 target element permitted determination of the unknown ^{31}P(n,p) cross section by comparison with the known ^{1}H(n,p) cross section.

The emerging protons were momentum analyzed in the TRIUMF Second Arm SPectrometer (SASP) [18]. SASP is a 110 ton Q-Q-D magnetic spectrometer with an acceptance of 13 msr and a momentum bite of 25%. The SASP detector

system comprised a focal plane detector package and a front-end detector package. The focal plane detector package consisted of a pair of drift chambers (VDC1 and VDC2) followed by a segmented scintillator array (PD0-PD4) and a large monolithic scintillator (S1). The front-end detector package consisted of a pair of drift chambers (FEC0 and FECM) followed by a trigger scintillator (FET). The event trigger was the AND of front-end and focal plane triggers, where the front-end trigger demanded hits in the FET scintillator and each FEC wire plane and the focal plane trigger demanded hits in a PD scintillator, the VDC1 X plane, and the S1 scintillator. If the FEV scintillator was hit, the event trigger was rejected.

Data were collected at spectrometer settings of 0°, 3°, 5°, 10°, and 15° using a 110 mg/cm^2 thick ^{7}Li foil, and 15°, 20°, and 25° using a 220 mg/cm^2 thick ^{7}Li foil. The 110 mg/cm^2 data set yielded a somewhat better energy resolution and the 220 mg/cm^2 data set yielded a somewhat higher counting rate. Additionally, data were collected at each spectrometer setting with a $(CH_2)^6$ target arrangement (for acceptance studies) and a (Mylar)$^5 \cdot CH_2$ target arrangement (for background studies).

III. DIFFERENTIAL CROSS SECTIONS

A number of cuts and corrections were applied to the raw data. A segmented target cut required (i) a valid hit pattern in the target wire chambers (i.e., no chamber hits upstream, and contiguous chamber hits downstream, of the struck target), and (ii) a valid (x,y) coordinate at the target face (i.e., ensuring the particle trajectory originated from the P material, not the Al support). A particle identification cut required (i) proton time-of-flight between the FET and PD scintillators, and (ii) pulse height corresponding to proton energy loss in the PD scintillators. We also applied corrections for proton energy loss in the target assembly, slight variations of the SASP acceptance with the focal plane coordinates, and the low-energy tail of the neutron beam. Lastly, using the scattering angle determined by the FECs, the data were subdivided into 1°-wide bins between 0 and 5 degrees, 2°-wide bins between 5 and 15 degrees, and 3°-wide bins between 15 and 30 degrees.

The resulting (n,p) spectra include background events from the Mylar windows of the phosphorus targets. The Mylar background comprises a large peak from the ^{1}H(n,p) reaction, a small peak from the ^{12}C(n,p) reaction, and a weak continuum. At zero degrees the ^{1}H(n,p) is located at -0.7 MeV in the ^{31}Si spectrum. With increasing angle the ^{1}H(n,p) peak slides across the ^{31}Si spectrum. To subtract the Mylar background from the phosphorus spectrum we collected Mylar and phosphorus data at each spectrometer setting. The (Mylar)$^5 \cdot CH_2$ target stack data were normalized to the $(^{31}P)^5 \cdot CH_2$ target stack data both ''directly'' [using the ^{1}H(n,p) peak in the Mylar and phosphorus spectra] and ''indirectly'' [using the ^{1}H(n,p) peak in the CH_2 spectrum] as a consistency check on the subtraction procedure. Figure 1 shows the ^{31}P spectrum and Mylar background spectrum for the 0–1° data set.

Finally, the ^{31}P(n,p) spectra from the P target (elements 1–5) were normalized via the ^{1}H(n,p) peak from the CH_2 target (element 6). The use of the known ^{1}H(n,p) differential cross section to determine the unknown ^{31}P(n,p) differential cross section avoided the need to know the absolute neutron flux and the absolute spectrometer acceptance. The ^{1}H(n,p) differential cross section, at the appropriate energy and scattering angles, was computed using the solution SM97 of the phase shift analysis computer program SAID [19]. Table I lists the ^{31}P(n,p) differential cross section versus ^{31}Si excitation energy for the 0–1° data set.

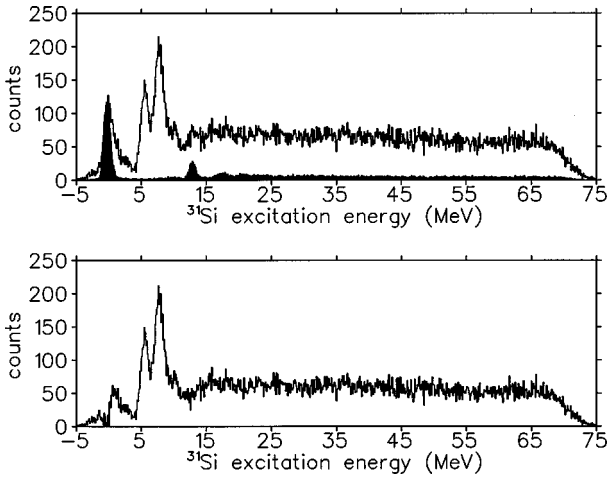

FIG. 1. The 0–1° ^{31}P(n,p) spectrum before (top) and after (bottom) the Mylar background subtraction. The shaded region in the upper plot is the appropriately normalized Mylar background spectrum. The larger Mylar peak at -0.7 MeV is due to the ^{1}H(n,p) reaction and the smaller Mylar peak is due to the ^{12}C(n,p) reaction.

IV. GAMOW-TELLER STRENGTH

To extract the GT strength distribution, and evaluate its uncertainty, we performed a multipole decomposition analysis (MDA) on the ^{31}P(n,p) cross section data (see Refs. [3,20]). In the MDA the measured differential cross sections

TABLE I. The ^{31}P(n,p) double differential cross section for the 0–1°. angular-bin and ^{31}Si excitation energies up to 27 MeV.

E_x (MeV)	$d^2\sigma/d\Omega dE$ (mb/sr MeV)	E_x (MeV)	$d^2\sigma/d\Omega dE$ (mb/sr MeV)
−2.0	0.29	13.0	0.94
−1.0	0.35	14.0	1.24
0.0	0.36	15.0	1.27
1.0	1.35	16.0	1.53
2.0	0.88	17.0	1.26
3.0	0.64	18.0	1.37
4.0	0.42	19.0	1.27
5.0	2.06	20.0	1.16
6.0	3.09	21.0	0.98
7.0	2.90	22.0	1.13
8.0	4.76	23.0	1.22
9.0	2.50	24.0	0.99
10.0	1.69	25.0	1.08
11.0	1.23	26.0	1.09
12.0	1.01	27.0	1.07

TABLE II. Summary of ^{31}P(n,p) multipole decomposition analyses options 1–8. The spin-parity multipoles and single particle transitions of different l values are identified by $(hole^{-1},\ particle)_{J^\pi}$.

Option	$l=0$	$l=1$	$l=2$	$l>2$	ΣB_{GT} $E_x<10$ MeV	ΣB_{GT} $E_x<15$ MeV
1	$(0d_{5/2}^{-1},0d_{3/2})_{1^+}$	$(0d_{3/2}^{-1},1p_{3/2})_{1^-}$ $(0d_{3/2}^{-1},1p_{3/2})_{0^-}$	$(1s_{1/2}^{-1},0d_{3/2})_{2^+}$	$(0d_{3/2}^{-1},1p_{3/2})_{3^-}$	2.32	2.62
2	$(0d_{5/2}^{-1},0d_{3/2})_{1^+}$	$(0d_{3/2}^{-1},1p_{3/2})_{1^-}$ $(0d_{3/2}^{-1},1p_{3/2})_{0^-}$	$(1s_{1/2}^{-1},0d_{3/2})_{2^+}$	$(0d_{5/2}^{-1},0d_{3/2})_{4^+}$	2.35	2.90
3	$(0d_{5/2}^{-1},0d_{3/2})_{1^+}$	$(0d_{3/2}^{-1},1p_{3/2})_{1^-}$ $(0d_{3/2}^{-1},1p_{3/2})_{0^-}$	$(1s_{1/2}^{-1},0d_{3/2})_{2^+}$	$(0d_{3/2}^{-1},0f_{7/2})_{5^-}$	2.36	2.96
4	$(0d_{5/2}^{-1},0d_{3/2})_{1^+}$	$(0d_{3/2}^{-1},1p_{3/2})_{1^-}$ $(0d_{3/2}^{-1},1p_{3/2})_{0^-}$	$(1s_{1/2}^{-1},0d_{3/2})_{2^+}$	$(0d_{3/2}^{-1},1p_{3/2})_{3^-}$ $(0d_{5/2}^{-1},0d_{3/2})_{4^+}$ $(0d_{3/2}^{-1},0f_{7/2})_{5^-}$	2.10	2.51
5	$(1s_{1/2}^{-1},1s_{1/2})_{1^+}$	$(0d_{3/2}^{-1},1p_{3/2})_{1^-}$ $(0d_{3/2}^{-1},1p_{3/2})_{0^-}$	$(1s_{1/2}^{-1},0d_{3/2})_{2^+}$	$(0d_{3/2}^{-1},1p_{3/2})_{3^-}$	2.36	2.68
6	$(0d_{5/2}^{-1},0d_{3/2})_{1^+}$	$(0d_{5/2}^{-1},0f_{7/2})_{1^-}$ $(0d_{3/2}^{-1},1p_{3/2})_{0^-}$	$(1s_{1/2}^{-1},0d_{3/2})_{2^+}$	$(0d_{3/2}^{-1},1p_{3/2})_{3^-}$	2.25	2.35
7	$(0d_{5/2}^{-1},0d_{3/2})_{1^+}$	$(0p_{3/2}^{-1},0d_{5/2})_{1^-}$ $(0d_{3/2}^{-1},1p_{3/2})_{0^-}$	$(1s_{1/2}^{-1},0d_{3/2})_{2^+}$	$(0d_{3/2}^{-1},1p_{3/2})_{3^-}$	2.17	2.20
8	$(0d_{5/2}^{-1},0d_{3/2})_{1^+}$	$(0d_{3/2}^{-1},1p_{3/2})_{1^-}$	$(1s_{1/2}^{-1},0d_{3/2})_{2^+}$	$(0d_{3/2}^{-1},1p_{3/2})_{3^-}$	2.37	2.84

$\sigma^{expt}(\theta)$ are fitted to summed theoretical angular distributions $\sigma_{J^\pi}^{theo}(\theta)$

$$\sigma^{expt}(\theta)=\sum_{J^\pi} \quad C_{J^\pi} \quad \sigma_{J^\pi}^{theo}(\theta) \tag{1}$$

of definite spin-parity transfer J^π. The coefficients C_{J^π} multiplying the theoretical curves $\sigma_{J^\pi}^{theo}(\theta)$ are determined by the ''best fit'' (with the obvious constraint $C_{J^\pi}\geqslant 0$). The fits of the summed theoretical angular distributions to the measured differential cross sections were performed for excitation energies from -5 MeV to $+25$ MeV in 1 MeV steps.

For ^{31}P(n,p) at $T_n=198$ MeV and $0°\leqslant\theta\leqslant 30°$ we expect contributions of orbital angular momenta $l<4$. In principle, each l value yields multipoles with $J=l-1,l$ and $l+1$, but generally, multipoles of different J but same l have similar shapes. The sets of spin-parity multipoles used in the multipole decomposition analyses are listed in Table II. In evaluating the sensitivity of the GT strength distribution to the MDA multipole set we found the choice of the $l=1$ curve (i.e., $J^\pi=0^-$ or $J^\pi=1^-$) had the greatest influence.

The angular distributions for the required multipoles were obtained via the distorted wave impulse approximation using the computer program DW83 [21]. The DWIA input were the projectile-target NN interaction, optical potential, and the one-body transition densities of the ^{31}P$\rightarrow^{31}$Si transitions. For the projectile-target NN interaction we used the t matrix of Franey and Love [22]. For the optical potential we used the ^{31}P matter distribution of de Vries *et al.* [23] folded with the projectile-target NN interaction using the computer program MAINX8 [24]. Lastly, for the ^{31}P$\rightarrow^{31}$Si one-body transitions densities we selected a variety of plausible single-particle (s.p.) transitions.

In selecting s.p. transitions for the different J^π multipoles our guide was to regard ^{31}P as a filled $0p$ shell, an empty $1p$-$0f$ shell, and 15 valence nucleons populating the $0d_{5/2}$, $1s_{1/2}$, and $0d_{3/2}$ orbitals. For the 1^+ multipole we computed angular distributions between all $1s$-$0d$ shell orbitals (consistent with the Gamow-Teller selection rules). We then ran the MDA with those shapes showing the greatest variations. For the 1^- multipole we computed angular distributions for all excitations from the $0p$ shell to the $1s$-$0d$ shell and from the $1s$-$0d$ shell to the $1p$-$0f$ shell (consistent with the dipole selection rules). We then ran the MDA with those shapes showing the greatest variations. For higher l-value multipoles, we employed similar approaches (Table II gives the complete set of s.p. transitions used). Lastly, studies of the sensitivity to the parameters of the NN interaction and optical potential, revealed negligible effects in the multipole decomposition.

The MDA determines the $J^\pi=1^+$ component of the measured cross section [denoted $\sigma_{1^+}(\theta)$]. To convert the cross section $\sigma_{1^+}(\theta)$ into the GT strength distribution B_{GT} we used

$$\sigma_{1^+}(0-1°)=\hat{\sigma} \quad f(q,\omega) \quad B_{GT} \tag{2}$$

where $\hat{\sigma}$ is the unit cross section and $f(q,\omega)$ corrects for the finite energy (ω) and momentum (q) transfer in the (n,p)

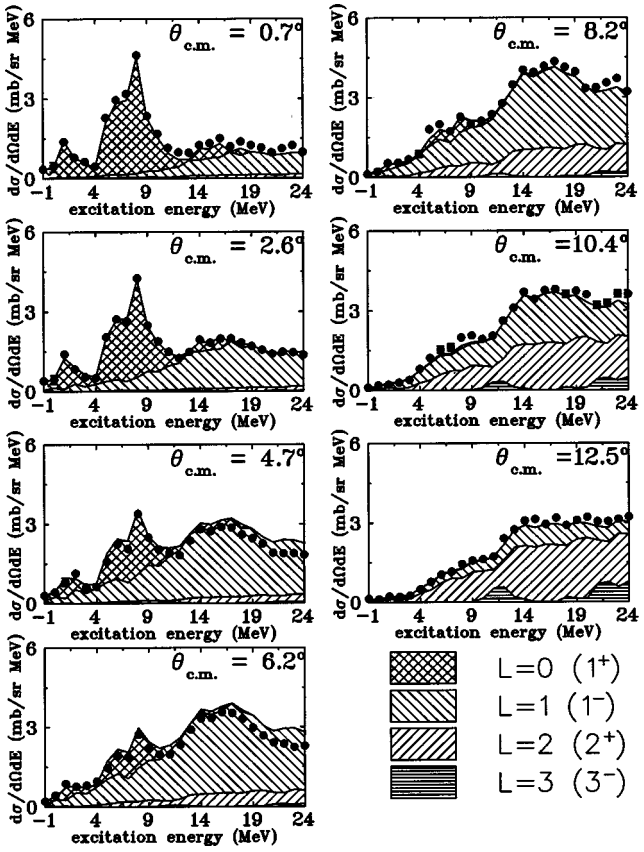

FIG. 2. Results of the ^{31}P(n,p) multipole decomposition analysis (option 1) showing the angular regions of the Gamow-Teller and dipole resonances. The spin-parity multipoles are identified according to $l(J^{\pi})$.

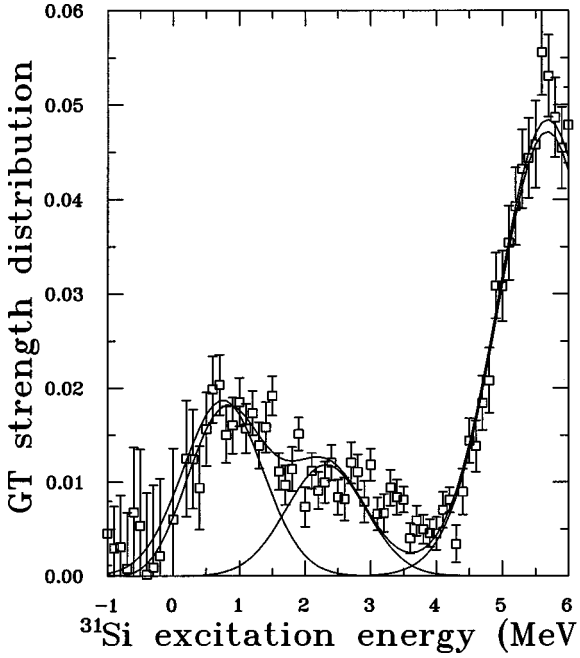

FIG. 3. Fit to the low-lying ^{31}Si levels in the measured GT strength distribution. The points are the experimental data and the solid lines are the ''best fit'' curve for the 0.75, 2.32, and ~5.0 MeV peaks.

reaction (note the B_{GT} units are such that $B_{\mathrm{GT}}=3$ for free neutron beta decay). The correction factor $f(q,\omega)$ was computed with the computer code DW83 and is within a few percent of unity. The unit cross section, $\hat{\sigma}=7.75\pm0.39$, was computed by extrapolating the measured unit cross section for $^{13}\mathrm{C}_{\mathrm{g.s.}}(n,p)^{13}\mathrm{B}_{\mathrm{g.s.}}$ [2] from $A=13$ to 31 using the empirical A dependence of Ref. [25]. Normally, the value of $\hat{\sigma}$ is generally taken from the ratio of the σ_{1^+} cross section and B_{GT} transition probability for analogous transitions in the target nucleus. Unfortunately, the very weak $^{31}\mathrm{Si}_{\mathrm{g.s.}}(\beta^-)^{31}\mathrm{P}_{\mathrm{g.s.}}$ beta decay ($B_{\mathrm{GT}}=0.012$ [26]), makes the proportionality of its (n,p) cross section and GT transition probability unreliable.

Table II lists the multipole sets, s.p. transitions, and GT strength sums, for the various multipole analyses performed (options 1–8). Figure 2 shows the J^{π} multipole assignments versus ^{31}Si excitation energy for MDA option 1. The peak at ~0° and ~7 MeV is clearly identified as Gamow-Teller in character and the peak at ~6° and ~15 MeV is clearly identified as dipole in character. Table II indicates the large quantity of GT strength below 10 MeV is essentially insensitive to the MDA option, whereas the small quantity of GT strength above 10 MeV varies significantly with the MDA option. The latter variations are mostly a result of sensitivity to different zero degree amplitudes of the various $l\geqslant1$ multipoles and s.p. transitions. The summed GT strength, using MDA option 1, is 2.32 ± 0.20 below 10 MeV and 2.62 ±0.23 below 15 MeV [the quoted uncertainty includes the statistical uncertainty in the MDA, the published uncertainty in the $^{13}\mathrm{C}_{\mathrm{g.s.}}(n,p)^{13}\mathrm{B}_{\mathrm{g.s.}}$ unit cross section, and an overall normalization uncertainty of ±7%].

V. B_{GT} VALUES FOR LOW-LYING LEVELS

Of importance to the muon capture investigations of the induced pseudoscalar coupling are the GT transition probabilities to ^{31}Si bound states ($E_x<5.8$ MeV). The relevant states are the $1/2^+$ ground state, the $1/2^+$, 0.75 MeV excited state, the $3/2^+$, 2.32 MeV excited state, and several $1/2^+$ and $3/2^+$ states near 5 MeV.

To extract the B_{GT} values for these GT transitions we fitted the -1 MeV$\leqslant E_x\leqslant$6 MeV region of the GT strength distribution to a series of peaks. We deployed one Gaussian for each level at 0, 0.75, and 2.32 MeV and another Gaussian for the level cluster at ~5 MeV [these states are unresolved in the (n,p) spectrum]. In fitting the 0, 0.75, and 2.32 MeV peaks, their centroids were fixed at their known excitation energies and their widths were fixed at the measured instrumental resolution (FWHM ~1.2 MeV) and only the amplitudes were varied. In fitting the ~5 MeV level cluster the peak centroid, width, and amplitude were all varied.

A concern in extracting the areas of the low-lying ^{31}Si peaks was the effects of subtracting the nearby $^{1}\mathrm{H}(n,p)$ peak. A sequence of fits, to determine the effects on the interesting ^{31}Si peaks of over or undersubtracting the background $^{1}\mathrm{H}(n,p)$ peak, were therefore performed. The resulting ''best fit'' curve and ''best fit'' B_{GT} values are given in Fig. 3 and Table III, respectively. The quoted uncertainties include: the statistical uncertainty in the fit, the published uncertainty in $\hat{\sigma}$ [2], the $^{1}\mathrm{H}(n,p)$ background subtraction uncertainty, and a ±7% overall normalization uncertainty.

TABLE III. B_{GT} values for ^{31}Si bound states. The experimental values are from the fit to the -1.0 MeV$\geq E_x \geq$6.0 MeV region of the measured GT strength distribution. The calculated values are from the $1s$-$0d$ shell model calculation using the universal SD residual interaction. The quoted experimental uncertainties include the statistical error in the fit, the published error in $\hat{\sigma}$, and a normalization error of 7%. The $\sim$5.0 MeV peak corresponds to several unresolved states.

E_x (MeV)	J^π	B_{GT}^{expt}	B_{GT}^{theo}
0.0	$3/2^+$	<0.10	0.052
0.75	$1/2^+$	0.26 ± 0.06	0.172
2.32	$3/2^+$	0.18 ± 0.03	0.097
$\sim$5.0		0.88 ± 0.13	

In the case of the weak transition to the ^{31}Si ground state we quote a B_{GT} upper limit.

VI. COMPARISON TO SHELL MODEL CALCULATIONS

Figure 4 compares the energy distribution and running sum of the ^{31}P$\rightarrow^{31}$Si GT strength from the multipole decomposition analysis and a shell model calculation. The experimental determination used the spin-parity multipoles and single-particle transitions of option 1 in Table II. The model calculation used the computer code OXBASH [27] with the full $1s$-$0d$ space and the universal SD interaction [26,28]. Figure 4 shows similar strength distributions for the measurement and calculation; both revealing a large, higher energy peak centered at $\sim$7 MeV, a small, lower energy peak centered at $\sim$1 MeV, and a weak continuum of GT strength from 10 to 15 MeV. The summed GT strength from 0 to 10 MeV are 2.32 ± 0.20 (expt.) and 3.33 (calc.) and from 0 to 15 MeV are 2.62 ± 0.23 (expt.) and 3.56 (calc.). In both cases,

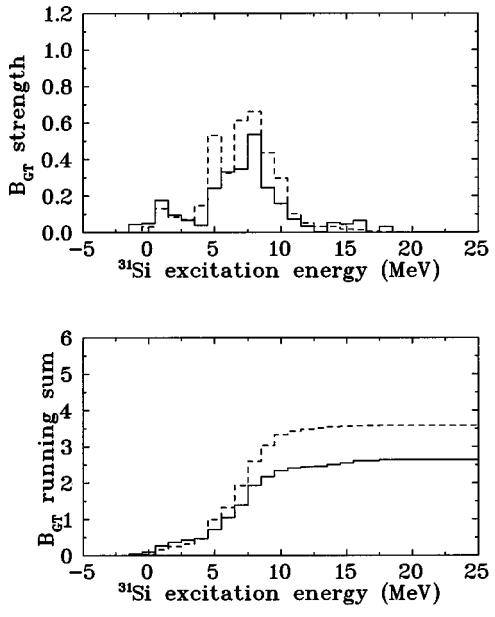

FIG. 4. The GT strength distribution (top) and the GT running sum (bottom) versus ^{31}Si excitation energy. The solid line is the (n,p) measurement and the dashed line is the shell model calculation with the full $1s$-$0d$ space and universal SD interaction.

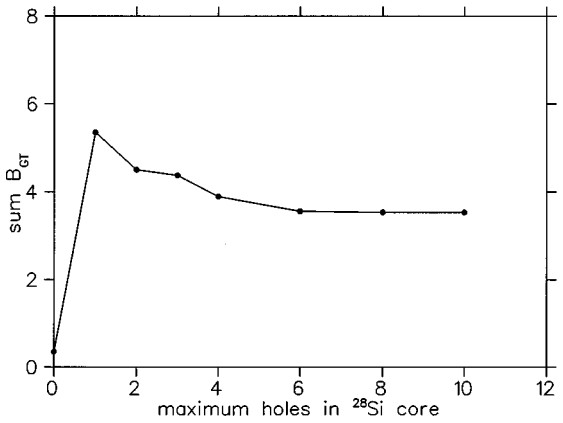

FIG. 5. Summed B_{GT} strength for ^{31}P$\rightarrow^{31}$Si versus the maximum number of allowed holes in the $0d_{5/2}$ core (using the universal SD interaction).

the ratio of measured strength to calculated strength is about 0.70. The ^{31}P$\rightarrow^{31}$Si reduction or quenching factor is typical of other charge exchange data on $1s$-$0d$ shell nuclei (e.g., Refs. [29,30]. It agrees with Siebels *et al.* for ^{23}Na(n,p) [15]—the only other published data for the (n,p) reaction on a $N>Z$ nucleus in the $1s$-$0d$ shell.

Table III compares the measured and calculated ^{31}P $\rightarrow^{31}$Si GT transition probabilities to low-lying ^{31}Si bound states. The pattern of GT transition probabilities in the data and the model are the same; the 0.75 MeV state B_{GT} value is largest, the 2.32 MeV state B_{GT} value is next, and the ground state B_{GT} value is smallest. However, contrary to the summed GT strength results, the experimental B_{GT} values are larger than the theoretical B_{GT} values for these low-lying levels. Most likely, since these states exhaust only a small fraction of the total strength, the model dependences of the calculated strengths is much greater for these individual B_{GT} values than the summed B_{GT} value. Other possible explanations are (i) the breakdown of proportionality between the (n,p) reaction and B_{GT} strength for weak transitions [25], and (ii) undersubtraction of the ^{1}H(n,p)-peak background (see Sec. V).

For $N>Z$ nuclei, configuration mixing via the residual interaction is more important (due to Pauli blocking) for the (n,p) reaction than the (p,n) reaction. As an illustration consider the $A=31$ nuclei as comprising a filled $0d_{5/2}$ core and three active nucleons in the $1s_{1/2}$-$0d_{3/2}$ orbitals, and the ^{31}P g.s. as comprising one proton and two neutrons in the $1s_{1/2}$ orbital. Then, GT transitions (via $1s_{1/2}\rightarrow 1s_{1/2}$ transitions) are allowed in the ^{31}P$(p,n)^{31}$S case but forbidden in the ^{31}P$(n,p)^{31}$Si case. Of course, in reality, configuration mixing admits hole states in the $0d_{5/2}$ and $1s_{1/2}$ orbitals and enables GT transitions in both (n,p) and (p,n) cases, but a greater sensitivity to configuration mixing is expected in the ^{31}P(n,p) reaction compared to the ^{31}P(p,n) reaction [28]. Figure 5 demonstrates the configuration mixing sensitivity of the ^{31}P$\rightarrow^{31}$Si total GT strength, showing the summed B_{GT} strength as a function of the maximum number of nucleon holes in the $0d_{5/2}$ core.

The sensitivity to configuration mixing is further corroborated by the calculations presented in Table IV. It lists B_{GT} sums for GT transitions from ^{31}P to $T_f=3/2$ states in ^{31}Si [the (n,p) direction] and $T_f=1/2$ states in ^{31}S [the (p,n)

TABLE IV. Comparison of B_{GT} sums computed using the full $1s$-$0d$ space and the empirical interaction of Wildenthal and Brown (denoted USD), the realistic interaction of Kuo (denoted KUO), and schematic modified surface-delta interaction (denoted MSD). The last column (Δ) is the difference of the largest and smallest calculated B_{GT} sum divided by the average of the calculated B_{GT} [e.g., for the first row $(5.769-1.455)/3.158=1.26$]. The larger the value of Δ, the poorer the agreement of the B_{GT} sums from the USD, KUO, and MSD interactions.

$i\rightarrow f$	$J_i\rightarrow J_f$	$T_i\rightarrow T_f$	ΣB_{GT}^{USD}	ΣB_{GT}^{KUO}	ΣB_{GT}^{MSD}	Δ
$^{31}P\rightarrow{}^{31}Si$	$1/2^+\rightarrow 1/2^+$	$1/2^+\rightarrow 3/2^+$	2.250	5.769	1.455	1.26
$^{31}P\rightarrow{}^{31}Si$	$1/2^+\rightarrow 3/2^+$	$1/2^+\rightarrow 3/2^+$	3.359	0.746	2.317	1.69
$^{31}P\rightarrow{}^{31}S$	$1/2^+\rightarrow 1/2^+$	$1/2^+\rightarrow 1/2^+$	3.327	1.826	2.417	0.59
$^{31}P\rightarrow{}^{31}S$	$1/2^+\rightarrow 3/2^+$	$1/2^+\rightarrow 1/2^+$	4.993	3.661	4.660	0.30

direction]. The B_{GT} sums were calculated using the full $1s$-$0d$ space and three different residual interactions: the empirical interaction of Brown and Wildenthal [26,28], the realistic interaction of Kuo [31], and the schematic modified surface delta interaction [32]. Table IV shows, for the summed B_{GT} strength, a much greater dependence on the residual interaction, implying a much greater sensitivity to configuration mixing, in the $^{31}P\rightarrow{}^{31}Si$ case than the $^{31}P\rightarrow{}^{31}S$ case. The consistency of the $^{31}P(n,p)$ quenching factor with other $1s$-$0d$ nuclei quenching factors, given the vital role of configuration mixing for the (n,p) reaction on $N>Z$ nuclei, represents a stringent quality test of the universal SD interaction.

VII. SUMMARY

In summary, using the charge exchange facility and the second arm spectrometer at TRIUMF, we have measured the $^{31}P(n,p)$ double differential cross section and extracted the $^{31}P\rightarrow{}^{31}Si$ Gamow-Teller strength distribution. A shell model calculation, using the full $1s$-$0d$ space and universal SD interaction, is in agreement with the measured GT distribution but over-estimates the total GT strength. The observed quenching factor of ~ 0.70 agrees with earlier measurements via $(p,n)/(n,p)$ reactions on other $1s$-$0d$ nuclei. Given the vital role of configuration mixing via the residual interaction on the $^{31}P\rightarrow{}^{31}Si$ GT strength, these data are a stringent test of the shell model. Lastly, the B_{GT} values corresponding to low-lying ^{31}Si states are important to investigations of the induced pseudoscalar coupling via the $^{31}P(\mu^-,\nu)$ muon capture reaction.

ACKNOWLEDGMENTS

We thank the TRIUMF technical staff for the smooth operation of the cyclotron, charge exchange facility and second arm spectrometer, and the National Science Foundation (U.S.) and the Natural Sciences and Engineering Research Council (Canada) for their financial support.

[1] C. D. Goodman, C. A. Goulding, M. B. Greenfield, J. Rapaport, D. E. Bainum, C. C. Foster, W. G. Love, and F. Petrovich, Phys. Rev. Lett. **44**, 1755 (1980).

[2] K. P. Jackson, A. Celler, W. P. Alford, K. Raywood, R. Abegg, R. E. Azuma, C. K. Campbell, S. El–Kateb, D. Frekers, P. W. Green, O. Hausser, R. L. Helmer, R. S. Henderson, K. H. Hicks, R. Jeppesen, P. Lewis, C. A. Miller, A. Moalem, M. A. Moinester, R. B. Schubank, G. G. Shute, B. M. Spicer, M. C. Vetterli, A. I. Yavin, and S. Yen, Phys. Lett. B **201**, 25 (1988).

[3] W. P. Alford and B. M. Spicer, Adv. Nucl. Phys. **24**, 1 (1998).

[4] M. C. Vetterli, O. Hausser, R. Abegg, W. P. Alford, A. Celler, D. Frekers, R. L. Helmer, R. Henderson, K. H. Hicks, K. P. Jackson, R. G. Jeppesen, C. A. Miller, K. Raywood, and S. Yen, Phys. Rev. C **40**, 559 (1989).

[5] T. Ronnqvist, H. Conde, N. Olsson, E. Ramstrom, R. Zorro, J. Blomgren, A. Hakansson, A. Ringbom, G. Tibell, O. Jonsson, L. Nilsson, P.-U. Renberg, S. Y. van der Werf, W. Unkelbach, and F. P. Brady, Nucl. Phys. **A563**, 225 (1993).

[6] S. El-Kateb, K. P. Jackson, W. P. Alford, R. Abegg, R. E. Azuma, B. A. Brown, A. Celler, D. Frekers, O. Hausser, R. L. Helmer, R. S. Henderson, K. H. Hicks, R. Jeppesen, J. D. King, K. Raywood, G. G. Shute, B. M. Spicer, A. Trudel, M. Vetterli, and S. Yen, Phys. Rev. C **49**, 3128 (1994).

[7] J. Rapaport, T. Taddeucci, P. Welch, C. Gaarde, J. Larsen, C. Goodman, C. C. Foster, C. A. Goulding, D. Horen, E. Sugarbaker, and T. Masterson, Phys. Rev. Lett. **47**, 1518 (1981).

[8] W. P. Alford, A. Celler, B. A. Brown, R. Abegg, K. Ferguson, R. Helmer, K. P. Jackson, S. Long, K. Raywood, and S. Yen, Nucl. Phys. **A531**, 97 (1991).

[9] A. Frischknecht, M. Dobeli, W. Stehling, G. Strassner, P. Troul, J. C. Alder, C. Joseph, J. F. Loude, J. P. Perroud, D. Ruegger, M. T. Tran, and H. Panke, Phys. Rev. C **38**, 1996 (1988).

[10] D. S. Armstrong, S. Ahmad, R. A. Burnham, T. P. Gorringe, M. D. Hasinoff, A. J. Larabee, C. E. Waltham, G. Azuelos, J. A. Macdonald, J-M. Poutissou, M. Blecher, D. H. Wright, E. T. H. Clifford, J. Summhammer, P. Depommier, R. Poutissou, H. Mes, and B. C. Robertson, Phys. Rev. C **40**, 1100 (1989).

[11] D. S. Armstrong, A. Serna-Angel, S. Ahmad, G. Azuelos, W. Bertl, M. Blecher, C. Q. Chen, P. Depommier, T. von Egidy, T. P. Gorringe, M. D. Hasinoff, R. S. Henderson, A. J. Larabee, J. A. Macdonald, S. C. McDonald, J-M. Poutissou, R. Poutissou, B. C. Robertson, D. G. Sample, G. N. Taylor, D. H.

Wright, and N. S. Zhang, Phys. Rev. C **46**, 1094 (1992).
[12] T. P. Gorringe, B. Johnson, D. S. Armstrong, J. Bauer, M. A. Kovash, M. D. Hasinoff, D. F. Measday, B. A. Moftah, R. Porter, and D. H. Wright, Phys. Rev. Lett. **72**, 3472 (1994); Phys. Rev. C **54**, 2714 (1996).
[13] V. Brudanin *et al.*, Nucl. Phys. **A587**, 477 (1995).
[14] B. A. Moftah, E. Gete, D. F. Measday, D. S. Armstrong, J. Bauer, T. P. Gorringe, B. L. Johnson, B. Siebels, and S. Stanislaus, Phys. Lett. B **395**, 157 (1997).
[15] B. Siebels, T. P. Gorringe, W. P. Alford, J. Bauer, J. Evans, S. El-Kateb, K. P. Jackson, A. Trudel, and S. Yen, Phys. Rev. C **52**, 1488 (1995).
[16] TRIUMF proposal E674, ''Allowed and forbidden muon capture rates on $1s$-$0d$ shell nuclei,'' spokesperson: T. P. Gorringe, 1993.
[17] R. S. Henderson, W. P. Alford, D. Frekers, O. Hausser, R. L. Helmer, K. H. Hicks, K. P. Jackson, C. A. Miller, M. C. Vetterli, and S. Yen, Nucl. Instrum. Methods Phys. Res. A **257**, 97 (1987).
[18] P. L. Walden *et al.*, Nucl. Instrum. Methods A (to be published).
[19] R. A. Arndt and L. D. Soper, Scattering Analysis Interactive Dail-in (SAID) Program (SM90) (unpublished); R. A. Arndt *et al.*, Phys. Rev. D **45**, 3995 (1992).
[20] M. A. Moinester, Can. J. Phys. **65**, 660 (1987).
[21] R. Schaeffer and J. Raynal, Computer code DWBA70, extended version DW83, J. R. Comfort, Arizona State University, 1984 (unpublished).
[22] M. A. Franey and W. G. Love, Phys. Rev. C **31**, 488 (1985).
[23] H. de Vries, C. W. de Jager, and C. de Vries, At. Data Nucl. Data Tables **36**, 495 (1987).
[24] Computer code MAINX8, written by T. Cooper, modified by R. G. Jeppesen (unpublished).
[25] T. N. Taddeucci, C. A. Goulding, T. A. Carey, R. C. Byrd, C. D. Goodman, C. Gaarde, J. Larsen, D. Horen, J. Rapaport, and E. Sugarbaker, Nucl. Phys. **A469**, 125 (1987).
[26] B. A. Brown and B. H. Wildenthal, At. Data Nucl. Data Tables **33**, 347 (1985).
[27] B. A. Brown, A. Etchegoyen, W. D. M Rae, and N. S. Godwin, The Oxford-Buenos-Aires-MSU shell model code (OXBASH), MSUCL Report No. 524, 1986.
[28] B. H. Wildenthal, in *Progress In Particle and Nuclear Physics*, edited by D. H. Wilkinson, (Pergamon Press, Oxford, 1984).
[29] B. D. Anderson, T. Chittrakarn, A. R. Baldwin, C. Lebo, R. Madey, P. C. Tandy, J. W. Watson, C. C. Foster, B. A. Brown, and B. H. Wildenthal, Phys. Rev. C **36**, 2195 (1987).
[30] B. D. Anderson, N. Tamimi, A. R. Baldwin, M. Elaasar, R. Madey, D. M. Manley, M. Mostajabodda'vati, J. W. Watson, W. M. Zhang, and C. C. Foster, Phys. Rev. C **43**, 50 (1991).
[31] T. T. S. Kuo, Nucl. Phys. **A103**, 71 (1967).
[32] B. H. Wildenthal, J. B. McGrory, E. C. Halbert, and H. D. Graber, Phys. Rev. C **4**, 1708 (1971).